IEEE Access
Multidisciplinary ⋮ Rapid Review ⋮ Open Access Journal

Received October 19, 2020, accepted October 27, 2020, date of publication October 30, 2020, date of current version November 11, 2020.

*Digital Object Identifier 10.1109/ACCESS.2020.3034968*

# A Hierarchical V2G/G2V Energy Management System for Electric-Drive-Reconstructed Onboard Converter

**SHUO LIU[1], DIXI XIN[1], LIYONG YANG[2], JIANLIN LI[1], (Member, IEEE), AND LI WANG[1], (Member, IEEE)**

[1]Electrical and Control Engineering College, North China University of Technology, Beijing 100144, China
[2]Beijing Electric Power Energy-Saving Key Technology Collaborative Innovation Center, North China University of Technology, Beijing 100144, China

Corresponding author: Dixi Xin (2018311010111@mail.ncut.edu.cn)

This work was supported in part by the National Natural Science Foundation of China under Grant 51807001 and in part by the Beijing Council of Science and Technology under Grant Z201100004520016.

**ABSTRACT** Due to the popularity of plug-in electric vehicles (PEV)and the development of converter technology, the electric-drive-reconstructed onboard converter(EDROC)is widely used in the charging system which can work in vehicle to grid(V2G) mode or grid to vehicle(G2V) mode. In this article, an EDROC for V2G/G2V energy management system is proposed. The EDROC uses permanent magnet synchronous motor as a charging inductor in V2G/G2V mode without additional equipment. Meanwhile, this article proposes a hierarchical V2G/G2V energy management system and the corresponding hierarchical control strategy with the proposed EDROC. This system can realize the energy distribution between PEVs, and avoid PEV overcharging. The proposed EDROC and control strategy are verified by simulation and experiment.

**INDEX TERMS** Vehicle-to-grid, hierarchical control strategy, plug-in electric vehicles, electric-drive-reconstructed onboard converter.

## I. INTRODUCTION

With the Plug-in electric vehicles (PEV) sales are rising, the PEVs are the most likely alternatives to combustion-engine vehicles [1]. Compared with other new energy vehicles (such as hybrid electric vehicles), the PEV has larger storage batteries which make the PEV suitable for participate in the vehicle to grid (V2G) or grid to vehicle (G2V) energy management. The technology of V2G/G2V can be used for load leveling and emission reduction [2], [3]. And the V2G/G2V systems are divided into three levels based on charging power level: Level 1 (convenience), Level 2 (primary), and Level 3 (fast) [4]. In Level 2 and Level 3, charging piles connect to the grid, which increases the hardware cost of V2G/G2V technology. The PEV working in Level 1 does not require additional charging equipment which is more suitable for participating in grid control.

The electric-drive-reconstructed onboard converter (EDROC) is proposed as the charger of PEV [5]. The EDROC reduces the volume and increases the power density by using the permanent magnet synchronous motor(PMSM) as the charging inductors for a charger. The charging or discharging power in V2G/G2V mode is less than the rated power in drive mode. And because the EDROC has not additional charging equipment, it is usually connected to the grid with the same transformer as the baseload and operates as in Level 1[6]. The structure of PEVs and baseload connected to the grid is shown in FIGURE 1, Each baseload contains one or more PEVs with EDROCs, and the base loads in the zone are connected to the grid through the same transformer.

However, the disorderly charging of PEV causes the additional charging load which's peak and the peak of baseload occurs at the same time. And the V2G/G2V energy management can effectively reduce the peaks of load with PEV [7]–[10] Generally, the hierarchical control system is applied to V2G/G2V including PEVs [11]. In this system, several PEVs share a power aggregator to form a subsystem., and the hierarchical system includes one or more power aggregators subsystem. The hierarchical systems are divided into three levels: grid-level, power aggregator-level,

The associate editor coordinating the review of this manuscript and approving it for publication was Christopher H. T. Lee.

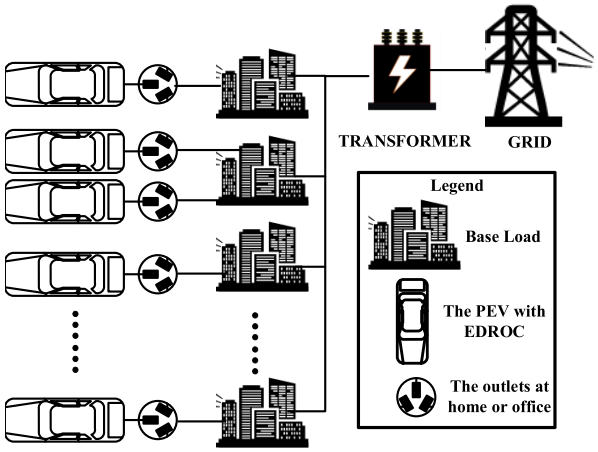


**FIGURE 1.** The structure of PEVs and baseload connected to the grid.

and vehicle-level. At the grid-level, energy flows between the grid and the aggregators. Considering that the V2G/G2V system operates in the home or office, the reactive power of the baseload can be compensated with the aggregator which operates at the grid-level [12].

For the V2G/G2V system which contains large-scale PEVs, the aggregator-level control strategy mainly relies on the parking model or online scheduling model for energy distribution [13]. The aggregator-level distribution scheme of the V2G/G2V energy management system with solar energy is discussed in [12]–[14]. In paper [15], a scheme based on the game-theoretical approach that can bring benefits to service providers and consumers is proposed. The paper [16] optimizes the system model from the perspective of pricing, improves the economic effect of the V2G/G2V system. The papers [17] and [18] study the communication reliability of the online scheduling model, reduce the error between online scheduling and actual demand. However, the parking model and online scheduling model are usually not applicable to the hierarchical system without large-scale PEVs (such as at home or office).

For the vehicle-level control strategy, the P-Q theory is used to control the active power and reactive power, respectively. In G2V mode, the PEV converter extracts active power from the grid to charge the battery; In V2G mode, the PEV battery provides active power to the grid through the converter [19]. For the V2G/G2V system works with the microgrid, the adaptive droop control based on the state of charge (SOC) is proposed in [20] and [21]. For charging stations with a large number of PEV, the droop control based on synchronous converter technology is proposed in [22]. The V2G/G2V converter work in Level 1 uses the vehicle-level control strategy to achieve excellent reactive power compensation capability [23].

In this article, an EDROC and corresponding hierarchical control strategy are proposed. The proposed EDROC applies the inductance of the PMSM as the charging inductor by an auxiliary circuit. The proposed EDROC system can use the socket at home or office to take participate in V2G/G2V. The hierarchical control strategy can realize the energy distribution between PEVs. The peaks of load and transformer capacity reduced by the proposed control strategy. Meanwhile, the hierarchical control strategy can independently operate without the parking model. The performance of the proposed EDROC and control strategy is verified through simulation and experimental results.

## II. TOPOLOGY AND ANALYSIS OF EDROC IN V2G

### A. THE TOPOLOGY OF THE PROPOSED EDROC

The electric-drive-reconstructed onboard converter (EDROC) is proposed, as shown in FIGURE 2, which combines the charging and driving system to increase power density by adding auxiliary circuits to the driver hardware. This topology is used in this article to investigate the hierarchical control strategy.

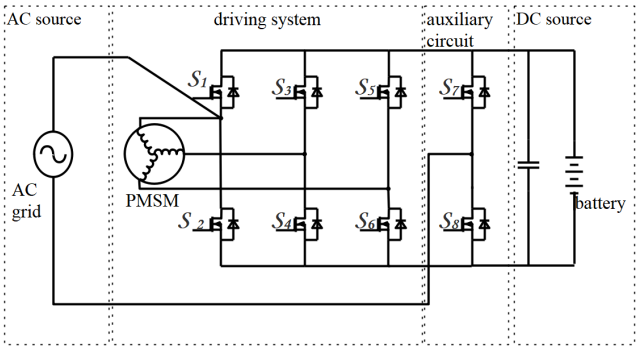


**FIGURE 2.** The topology of electric-drive-reconstructed converter.

### B. THE OPERATING STATE OF THE EDROC IN THE V2G/G2V MODE

In the V2G/G2V mode, the switches $S_1$&$S_2$ are disabled and the switches $S_3$-$S_8$ are enabled, the work states are shown in FIGURE 3. The switching states are divided into two ways of four work states each.

The states I-IV are the way I. The states I&II are working in the positive grid. In state I, the switches $S_5$ and $S_8$ are turned on, the switches $S_4$, $S_6$, and $S_7$ are turned off, and current flows through the body diode of switch $S_3$ as shown in FIGURE 3(a). The state equation can be expressed as

$$\begin{cases} \dfrac{di_a}{dt} = \dfrac{2\,(V_B - V_{ac})}{3L_s} \\ \dfrac{di_b}{dt} = \dfrac{V_{ac} - V_B}{3L_s} \\ \dfrac{di_c}{dt} = \dfrac{V_{ac} - V_B}{3L_s} \end{cases} \tag{1}$$

where, $V_{ac}$ is the voltage of the AC source; $V_B$ is the voltage of the battery; $i_a i_b$ and $i_c$ are the three-phase inductor current, respectively. $L_s$ is the stator inductance of the PMSM.

In state II, the switches $S_4$, and $S_7$ are turned on, the switches $S_3$, $S_5$, and $S_8$ are turned off, and current

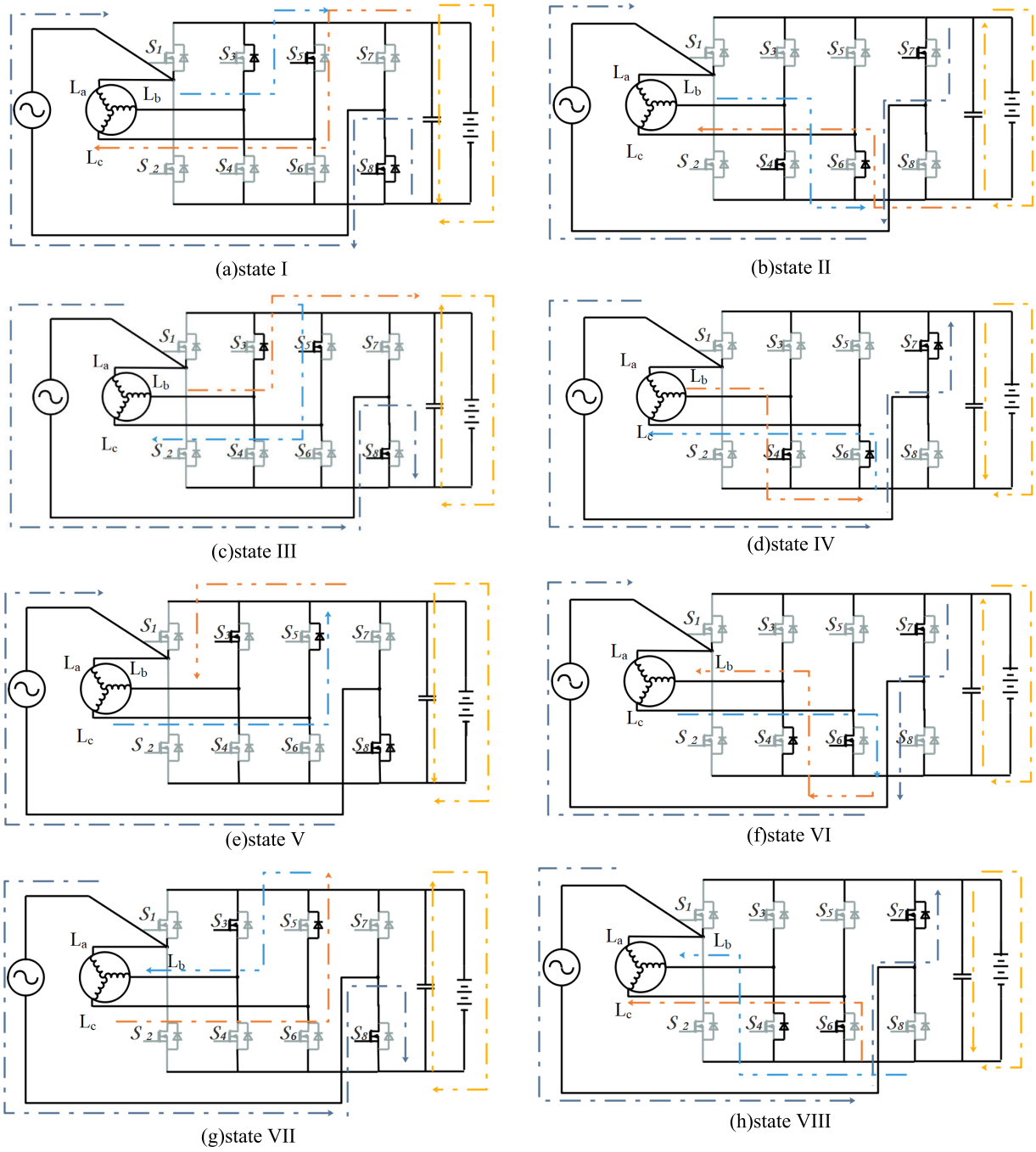


**FIGURE 3.** Switching states of the EDROC.

flows through the body diode of switch $S_6$ as shown in FIGURE 3(b). The state equation can be expressed as

$$\begin{cases} \dfrac{di_a}{dt} = \dfrac{2\left(-V_B - V_{ac}\right)}{3L_s} \\ \dfrac{di_b}{dt} = \dfrac{V_{ac} + V_B}{3L_s} \\ \dfrac{di_c}{dt} = \dfrac{V_{ac} + V_B}{3L_s} \end{cases} \tag{2}$$

The states III&IV are working in the negative grid, and the state equations are the same as that in the state I&II. The state equation can be expressed as

$$\begin{cases} \dfrac{di_a}{dt} = \dfrac{2\left(-V_B + V_{ac}\right)}{3L_s} \\ \dfrac{di_b}{dt} = \dfrac{-V_{ac} + V_B}{3L_s} \\ \dfrac{di_c}{dt} = \dfrac{-V_{ac} + V_B}{3L_s} \end{cases} \tag{3}$$

$$\begin{cases} \dfrac{di_a}{dt} = \dfrac{2\,(V_B + V_{ac})}{3L_s} \\ \dfrac{di_b}{dt} = \dfrac{-V_{ac} - V_B}{3L_s} \\ \dfrac{di_c}{dt} = \dfrac{-V_{ac} - V_B}{3L_s} \end{cases} \tag{4}$$

The states V-VIII are the way II. The way I and the way II work with the same state equation, and they can operate independently or alternately. The relationship between the AC voltage and the battery voltage can get:

$$\begin{cases} G = \frac{2}{1-D} \\ V_B = mGV_m \end{cases} \tag{5}$$

where $G$ is the voltage gain; $D$ is the duty cycle; $V_m$ is the amplitude of the voltage of the AC source; $m$ is the modulation index of the inverter.

### C. VEHICLE LEVEL CONTROL STRATEGY OF THE EDROC

In V2G/G2V mode, the control goal of the vehicle-level is regulating active and reactive power to meet the V2G/G2V system requirements. The operation area of V2G mode and G2V mode as shown in FIGURE 4. when the converter operates in V2G mode, the power flows from the PEV to the grid and it is operating in quadrant II or quadrant III; When the converter operates in G2V mode, the power flows from the grid to the PEV and it is operating in quadrant I or quadrant IV.

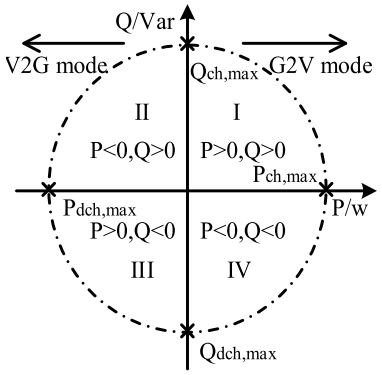


**FIGURE 4.** The operation area of V2G mode and G2V mode.

The setting of active and reactive power should lie within its capacity:

$$\begin{cases} -P_{dch,max} \le P^* \le P_{ch,max} \\ -Q_{dch,max} \le Q^* \le Q_{ch,max} \end{cases} \tag{6}$$

where, $P^*$ is the setting of the active power, $P_{dch,max}$ is the maximum active power discharge allowed to the converter, $P_{ch,max}$ is the maximum active power charge allowed to the converter; $Q^*$ is the setting of the reactive power, $Q_{dch,max}$ is the maximum reactive power discharge allowed to the converter, $Q_{ch,max}$ is the maximum reactive power charge for the converter.

The control strategies consist of three parts: the power controller, the battery voltage controller, and the AC current controller. The control block of the vehicle level is shown in FIGURE 5.

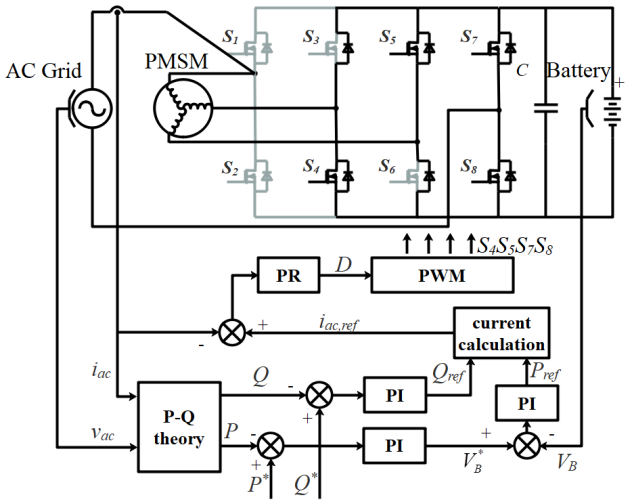


**FIGURE 5.** The proposed vehicle level control block.

The EDROC works as a converter with the constant output of active and reactive power in the V2G/G2V mode. The proposed control strategy obtains instantaneous power through the P-Q theory. The Sampling provides the $\alpha$ component AC grid and the single-phase phase-locked loop provides the $\beta$ component. The active power $P$ and reactive power $Q$ are obtained by Equation (7).

$$\begin{cases} P = v_\alpha * i_\alpha + v_\beta * i_\beta \\ Q = v_\beta * i_\alpha - v_\alpha * i_\beta \end{cases} \tag{7}$$

where, $v_\alpha$ and $v_\beta$ are the $\alpha$ and $\beta$ component of the AC voltage ($v_{ac}$), respectively; $i_\alpha$ and $i_\beta$ are the $\alpha$ and $\beta$ component of the AC current ($i_{ac}$), respectively.

The power controller is adjusted according to the active power setting ($P^*$) and reactive power setting ($Q^*$). The output of the power controller is the battery charging or discharging voltage reference ($V_B^*$) and reactive power reference $\left(Q_{ref}\right)$.The active power and reactive power are controlled by the PI controller, respectively. The transfer functions for the active power PI controller and reactive power PI controller are as follows:

$$\begin{cases} G_P(s) = K_P^P + \dfrac{K_i^p}{s} \\ G_Q(s) = K_P^Q + \dfrac{K_i^Q}{s} \end{cases} \tag{8}$$

where $K_P^P$, $K_i^P$ and $G_P(s)$ are the proportional constant, integral constant, and transfer function of the active power PI controller, respectively. $K_P^Q$, $K_i^Q$ and $G_Q(s)$ are the proportional constant, integral constant, and transfer function of reactive power PI controller, respectively.

The battery voltage controller controls the battery voltage via the PI controller. The given of the battery voltage controller is the output value of the power controller, and the output value of the battery voltage controller is the active power reference value ($P_{ref}$ ). The transfer functions for the PI controller are as follows:

$$G_B(s) = K_P^B + \frac{K_i^B}{s} \tag{9}$$

where $K_P^B$, $K_i^B$ and $G_B(s)$ are the proportional constant, integral constant, and transfer function of the battery voltage PI controller, respectively.

The input of the current calculation module is the active power reference value ($P_{ref}$) and the reactive power reference value $\left(Q_{ref}\right)$. The equations for the current calculation are as follows:

$$\begin{cases} \theta = \tan^{-1}\left(\dfrac{Q_{ref}}{P_{ref}}\right) \\ I_m = \dfrac{P_{ref}}{E_m \cos\theta} \\ i_{ac,ref} = I_m \sin(\omega t - \theta) \end{cases} \tag{10}$$

where $I_m$ and $E_m$ are the current and voltage amplitude of AC source, respectively; $\theta$ is the power factor angle; $i_{ac,ref}$ is the reference current of the AC source; $\omega$ is the angular frequency of the AC source.

The AC current controller is a PR controller so that the current of the AC grid can follow the reference value which is calculated by equation (10). The output of the AC current controller is a duty cycle(D). The transfer functions for the PR controller are as follows:

$$G_C(s) = K_P^C + \frac{2K_i^C \omega_c s}{s^2 + 2\omega_c s + \omega_o^2} \tag{11}$$

where, $K_P^C, K_i^C$ and $G_C(s)$ are the proportional constant, integral constant, and transfer function of the AC current PR controller, respectively. $\omega_o$ is the resonant angular frequency, $\omega_c$ is the crossover angular frequency.

The controller parameters are based on the bode diagram which is plotted in FIGURE 6. During designing the parameters of the control system, the design of the controller begins with the AC current PR controller. The resonant frequency is set with $314 rad/s$ which is the AC frequency of the proposed, and the crossover angular frequency is set as $\omega_c = 3 rad/s$[24]. The bandwidth of the battery voltage and power controller is below the resonant frequency to avoid instability of the AC current controller. Since the variation of the battery voltage is less than that of the AC source, the voltage controller is set with a larger bandwidth than that of the power controller. The active and reactive power controllers are set with different bandwidth so that the controllers do not conflict. The active power component is the main part of the total power in the V2G/G2V system, and enough phase margin of active power controller is beneficial to reduce the system overshoot.

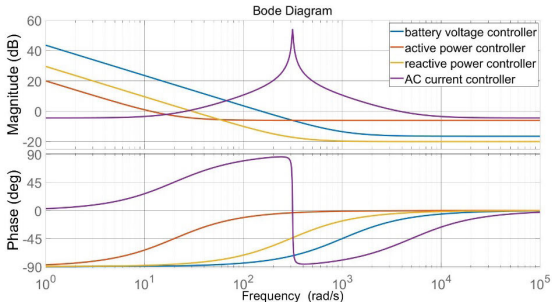


**FIGURE 6.** The bode diagram for the controllers.

## III. HIERARCHICAL V2G/G2V ENERGY MANAGEMENT SYSTEM WITH EDROC

### A. THE V2G/G2V ENERGY MANAGEMENT

During the operates time of PEV with EDROC, the baseload goes through one or more peaks and valley as the load curve with PEV[25] is shown in FIGURE 7. The EDROC has sufficient time to participate in load peaking through V2G/G2V energy management. The V2G/G2V energy management system regulates discharging (V2G) power and the charging(G2V) power of PEVs. When the load curve is at its peak, the energy management system regulates the charging power of the PEV to do as peak suppression. The PEVs with low SOC connected at this time should be charged at normal power. The PEVs with high SOC need to reduce charging power or even discharge to avoid overcharging. Overcharged PEVs need the department the system early. When the load curve is at its valley, the energy management system to increase charging power to do as valley filling.

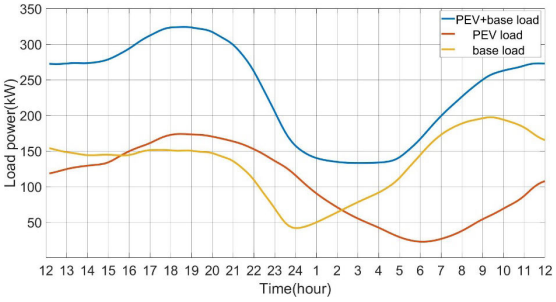


**FIGURE 7.** The power load curve with PEV.

### B. THE STRUCTURE OF HIERARCHICAL SYSTEM

The system structure and flowchart are shown in FIGURE 8 and FIGURE 9. The proposed system structure is divided into three parts: gird level, power aggregator level, and vehicle level. The baseload and power aggregator share a transformer which connected to the grid. Several PEVs share a power aggregator.

In the adjustment period of the V2G/G2V mode, the operating time which over a time horizon is divided into $K$ time slots and the duration of each time slot is $\Delta$t. In the time slot $k$, the PEV sends SOC data to the aggregator that uses the average value of PEVs SOC as the operation state, the

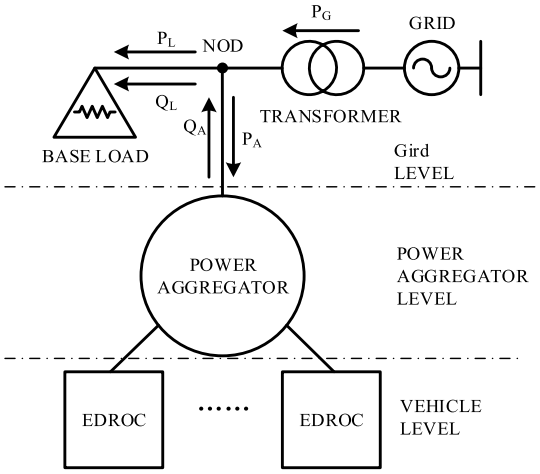


**FIGURE 8.** The system structure in V2G/G2V mode.

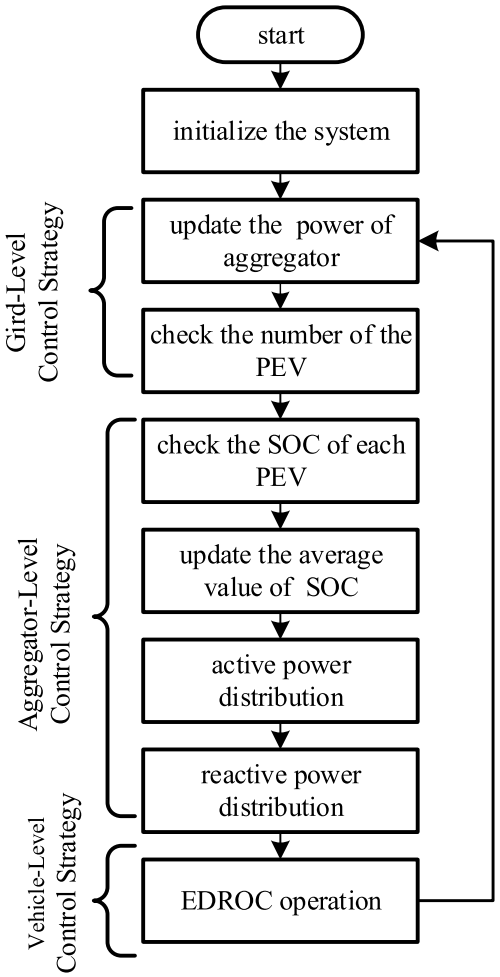


**FIGURE 9.** The flowchart of the hierarchical V2G/G2V system.

equation is as follows

$$s(k) = \frac{1}{N}\sum_{n=1}^{N} s_n(k) \tag{12}$$

where $\bar{s}(k)$ is the average value of SOC under the aggregator at time slot k;$s_n(k)$ is the SOC of PEV n at time slot $k$.

### C. POWER AGGREGATOR-LEVEL CONTROL STRATEGY

The aggregator-level controller sends active power reference and reactive power reference to each PEV. The control objective is reducing the dispersion of the SOC between each PEV to achieve a reasonable distribution of energy under the aggregator. The V2G/G2V system with the control objective can avoid PEV overcharge and reduce the fluctuation V2G/G2V total power. To express the degree of dispersion of the SOC, the objective function is formulated as (13).

$$\begin{aligned} F(s_1(k), s_2(k) \cdots s_N(k)) &= \frac{1}{N}\sum_{n=1}^{N} \left|\delta_n(k)\right| \\ &= \frac{1}{N}\sum_{n=1}^{N} \left|s_n(k) - (k)\right| \end{aligned} \tag{13}$$

where $\delta_n(k)$ is the deviation from the value of PEVs SOC at time slot k. Assuming that the total number of PEVs is $N$, and the battery specifications of these PEVs are the same. The aggregator-level control objectives were decided based on equation (14).

$$\min_{k=K} \left(F(s_1(k), s_2(k) \cdots s_N s(k))\right) \tag{14}$$

Considering the SOC limitation of PEV($S_{lim}$) and enough operation time, the control objectives decided based on the following equation:

$$\begin{cases} k \to \infty, \bar{s}(k) \to s_{lim} \\ p_1(k) = p_2(k) = \cdots = p_n(k), \\ F(s_1(k), s_2(k) \cdots s_N(k)) = 0 \end{cases} \tag{15}$$

The state equation of the aggregator-level control is shown as equation (16). The state variables are the SOC of each PEV and the average value of PEVs SOC, and the observation variable is the SOC dispersion The active power allocated to each PEV is used as an input variable.

$$\begin{cases} \mathbf{x}(\mathbf{k}+1) = \begin{bmatrix} 1 & 0 & \cdots & 0 & 0 \\ 0 & 1 & \cdots & 0 & 0 \\ \vdots & \vdots & \ddots & 0 & \vdots \\ 0 & 0 & \cdots & 1 & 0 \\ \frac{1}{N} & \frac{1}{N} & \cdots & \frac{1}{N} & 0 \end{bmatrix} \\ \quad \mathbf{x}(\mathbf{k}) + \begin{bmatrix} \lambda_{ch} & 0 & \cdots & 0 \\ 0 & \lambda_{ch} & \cdots & 0 \\ \vdots & \vdots & \ddots & \vdots \\ 0 & 0 & \cdots & \lambda_{ch} \\ \frac{\lambda_{ch}}{N} & \frac{\lambda_{ch}}{N} & \cdots & \frac{\lambda_{ch}}{N} \end{bmatrix} \mathbf{u}(\mathbf{k}) \\ \mathbf{y}(\mathbf{k}) = \begin{bmatrix} 1 & 0 & \cdots & 0 & -1 \\ 0 & 1 & \cdots & 0 & -1 \\ \vdots & \vdots & \ddots & 0 & \vdots \\ 0 & 0 & \cdots & 1 & -1 \end{bmatrix} \mathbf{x}(\mathbf{k}) \end{cases} \tag{16}$$

where,

$$\boldsymbol{x}(\boldsymbol{k}) = \begin{bmatrix} s_1(k) \\ s_2(k) \\ \vdots \\ s_n(k) \\ s(k) \end{bmatrix}, \quad \boldsymbol{u}(\boldsymbol{k}) = \begin{bmatrix} p_1(k) \\ p_2(k) \\ \vdots \\ p_n(k) \end{bmatrix},$$

$$\boldsymbol{y}(\boldsymbol{k}) = \begin{bmatrix} \delta_1(k) \\ \delta_2(k) \\ \vdots \\ \delta_n(k) \end{bmatrix},$$

$P_n(k)$ is the active power allocated by the PEV n at time slot k; $\lambda_{ch}$ is the battery efficiency, and it is defined as

$$\Delta S_n(k) = \lambda_{ch} P_n(k) \tag{17}$$

The aggregator-level control strategy is shown in FIGURE 10. Where $P_A(k)$ is the active power of aggregator which is controlled by gird-level control strategy; $\eta$ is the power balance parameter; $\mathbf{E}$ is the identity matrix. To meet the control objectives, the given of the observed variable is set to zero vector.

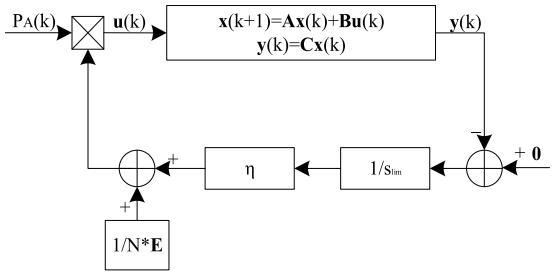


**FIGURE 10.** The aggregator-level control strategy.

The PEV under the aggregator gets the weight function used to allocate power as shown in equation (18) and the active power reference for each PEV is shown in equation (19). where, $f_n(k)$ is the power weight function allocated by the PEV n at time slot k which is regulated by the deviation of PEV and the power balance parameter; $\eta$ is the power balance parameter which adjusts the range of the active power reference.

$$\begin{cases} f_1(k) = \dfrac{1}{N} + \eta \dfrac{(0 - \delta_1(k))}{s_{lim}} \\ \vdots \\ f_n(k) = \dfrac{1}{N} + \eta \dfrac{(0 - \delta_n(k))}{s_{lim}} \end{cases} \tag{18}$$

$$\begin{cases} P_1(k) = (\dfrac{1}{N} + \eta \dfrac{(0 - \delta_1(k))}{s_{lim}}) P_A(k) \\ \vdots \\ P_n(k) = (\dfrac{1}{N} + \eta \dfrac{(0 - \delta_n(k))}{s_{lim}}) P_A(k) \end{cases} \tag{19}$$

Under the proposed aggregator-level control strategy, PEVs with higher SOC get a smaller weight function and PEVs with lower SOC get a larger weight function. In this way, the charging process of the PEV with high SOC is prolonged to avoid the PEV overcharging, and the charging process of PEVs with low SOC is shortened to reduce the PEV deviation.

Considering the range values of the distribution function, the maximum and minimum values of the active power according to the proposed control strategy are shown as equation (20).

$$\begin{cases} P_{n,max}(k) = \dfrac{1}{N} P_A(k) + \eta P_A(k) \\ P_{n,min}(k) = \dfrac{1}{N} P_A(k) - \eta P_A(k) \end{cases} \tag{20}$$

Moreover, the active power allocated to the PEV n at time slot k $P_n(k)$ should lie within its capacity:

$$P_{PEV,min} \le P_n(k) \le P_{PEV,max} \tag{21}$$

The relationship between the capacity of power and operating mode of PEV is shown as equation (22).

$$\begin{cases} P_{PEV,max} \ge 0, P_{PEV,min} \ge 0 G2V \\ P_{PEV,max} \ge 0, P_{PEV,min} < 0 V2G/G2V \\ P_{PEV,max} < 0, P_{PEV,min} < 0 G2V \end{cases} \tag{22}$$

where $P_{PEV,max}$ is the upper limit of the capacity of PEVs; $P_{PEV,min}$ is the lower limit of the capacity of PEVs.

Considering the capacity of power, the value range of the power balance parameter coefficient is as equation (23)

$$0 \le \eta \le min\left(\frac{P_{PEV,max}}{P_A(k)} - \frac{1}{N}, \frac{1}{N} - \frac{P_{PEV,min}}{P_A(k)}\right) \tag{23}$$

To ensure consistent the power factor angle of all PEVs under aggregator, the reactive power is distributed according to the distribution ratio of the active power, as shown in equation (23).

$$\begin{cases} Q_1(k) = \frac{P_1(k)}{P_A(k)} Q_A(k) \\ \vdots \\ Q_n(k) = \frac{P_n(k)}{P_A(k)} Q_A(k) \end{cases} \tag{24}$$

where $Q_n(k)$ is the reactive power allocated by the PEV n at time slot $k$; $Q_A(k)$ is the reactive power of the aggregator at time slot $k$.

The active and reactive power reference which distributed by the aggregator-level controllers is sent to PEVs as the given of vehicle-level controllers, respectively.

### D. GIRD-LEVEL CONTROL STRATEGY

The grid-level control objective is to compensate for the reactive power of baseloads, distribute active and reactive

power to the aggregator. The node balance of the grid-level control strategy is shown in equation (25).

$$\begin{cases} P_N(k) = P_G(k) - P_A(k) - P_L(k) \\ Q_N(k) = Q_A(k) - Q_L(k) \end{cases} \tag{25}$$

where, $P_N(k)$ and $Q_N(k)$ are the active and reactive power flowing through the node at time slot $k$, respectively. Ideally, the energy flowing through the node is zero. $P_L(k)$ and $Q_L(k)$ are the active and reactive power consumed by the baseload at time slot $k$, respectively; $P_A(k)$ and $Q_A(k)$ are the active and reactive power of the aggregator at time slot k, respectively.

After determining the distribution power of the grid-level, the active power requirements of the aggregator are determined. Considering the limitation of SOC and the current state of charge, the active power requirement is determined by equation (25). The function decreases as the average SOC grows so that the final average SOC is close to the SOC limit. [11]

$$P_A(k+1) = \frac{s_{lim-(k)}}{s_{lim}} P_{A,max} \tag{26}$$

where $S_{lim}$ is the maximum SOC limit of the PEV. $P_{A,max}$ is the upper limit of the capacity of the aggregator and defined as:

$$P_{A,max} = NP_{PEV,max} \tag{27}$$

## IV. SIMULATION AND EXPERIMENTAL RESULTS

### A. SIMULATIONS RESULTS

To verify the proposed system, a hierarchical V2G/G2V energy management system containing six PEVs are simulated. The simulation considers a 10-hour scheduling time which divides it into 120 time periods, each lasting 5 minutes. The power limit capacity of each PEV is set to 10KW. The limit of SOC is set to 80%. The simulated scene is shown in FIGURE 11. At the initial moment (12:00), the PEV1-5 is charged through the outlets at home or office. After 4-hour of the initial moment (16:00), the PEV5 leave from the outlet. After 6-hour of the initial moment (18:00), the PEV6 plug-in the outlet. In the simulated, all PEV controlled with the proposed hierarchical control strategy.

When the power balance parameter $\eta$ is set to 1.5, the PEVs are only allowed to work in the G2V mode. FIGURE 12 shows the active power of PEV during scheduling time; FIGURE 13 shows the SOC of PEV during scheduling time. At the initial moment (12:00), the deviations of the SOC of PEV1-PEV5 are 10.5%, 8.0%, 2.0%, 7.0%, 9.5%, respectively. The PEV1 is distributed to a power of 6.6 kW which is the maximum power in the system. The PEV5 is distributed to a power of 0.4 kW which is the minimal power in the system. After 4 hours of initial moment (16:00), the deviations of the SOC of PEV1- PEV5 are 1.6%, 1.2%, 0.3%, 1.0%, 1.4%, respectively. The dispersion of SOC is reduced from the initial state. After PEV5 departure at the fourth hour (16:00) and PEV6 was plug-in at the sixth hour (18:00), the SOC of PEV did not fluctuate. At the final moment, every PEVs in the system are not overcharged.

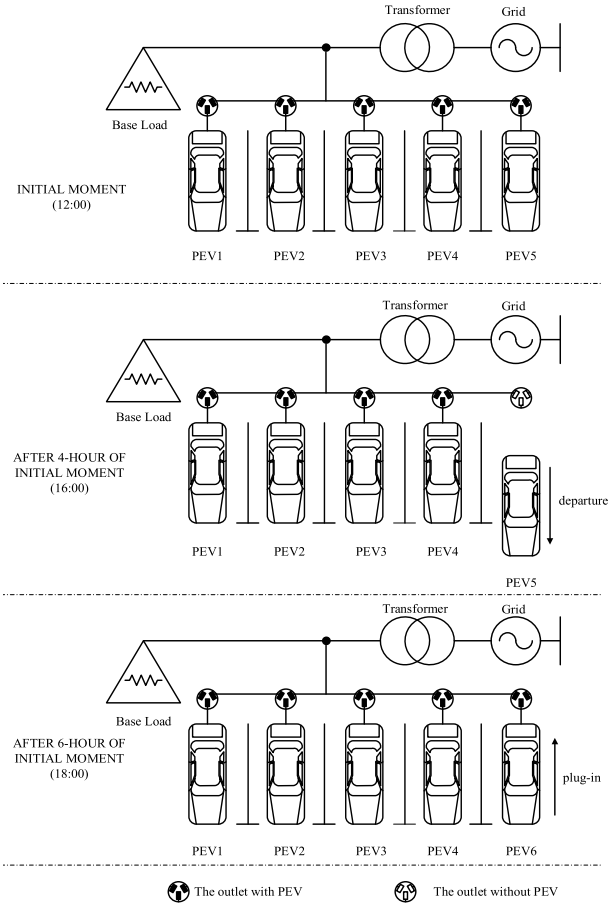


**FIGURE 11.** The simulated scene for hierarchical System.

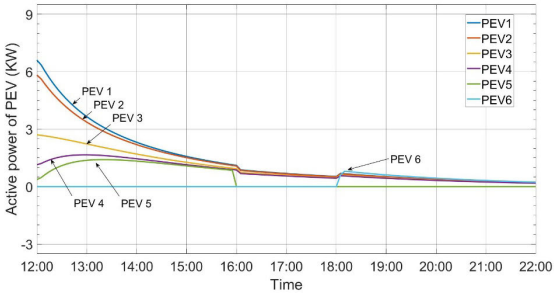


**FIGURE 12.** Active power of PEV work in G2V mode.

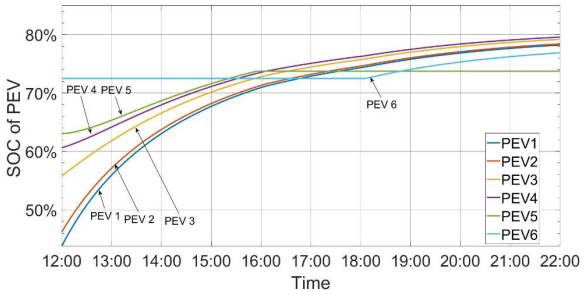


**FIGURE 13.** SOC of PEV work in G2V mode.

When the power balance parameter $\eta$ is set to 2.5, the PEVs are allowed to work in G2V mode or V2G mode, FIGURE 14

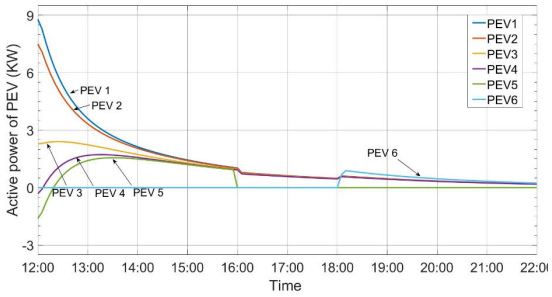


**FIGURE 14.** Active power of PEV work in G2V/V2G mode.

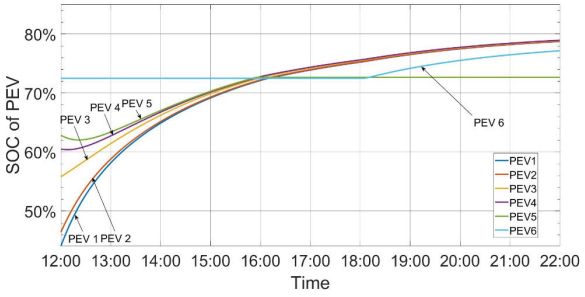


**FIGURE 15.** SOC of PEV work in G2V/V2G mode.

shows the active power of PEV during scheduling time; FIGURE 15 shows the SOC of PEV during scheduling time. In this simulation, the initial state of PEV is the same as the simulation which is only allowed to work in the G2B mode. At the initial moment (12:00), the PEV1 is distributed to a power of 8.8 kW which is the maximum power in the system. The PEV5 is distributed to the power of -1.6 kW which is the minimal power in the system. The values range of the power in this simulation is wider than that in the simulation which is only allowed to work in G2V mode. Because PEV4 and PEV5 have a high initial SOC and large deviation, their initial power is given a negative value while operating in V2G mode. Under the control strategy, the power given of PEV4&5 increases with the decrease of the deviation, and when the given of power changes from negative to positive, PEV4&5 changes from V2G mode to G2V mode. After 2 hours of initial moment (14:00), the deviations of the SOC of PEV1-PEV5 are 1.1%, 0.9%,0.2%, 0.7%, 1.0%, respectively. After 4 hours of initial moment (16:00), the deviations of the SOC of PEV1-PEV5 are 0.4%, 0.3%,0.1%, 0.2%, 0.4%, respectively. In this simulation, the dispersion of SOC is reduced more rapidly than the simulation which is only allowed to work in the G2V mode.

When the SOC of all PEVs are higher than the limit of SOC. the PEV only allowed to work in the V2G mode. In the simulation, the power balance parameter $\eta$ is set to 0.2 and the limit of SOC is set to 20%, the PEVs work in the V2G mode. FIGURE 16 shows the active power of PEV during scheduling time; FIGURE 17 shows the SOC of PEV during scheduling time.

FIGURE 18 shows the relationship between power balance parameter $\eta$ and objective function, the objective function

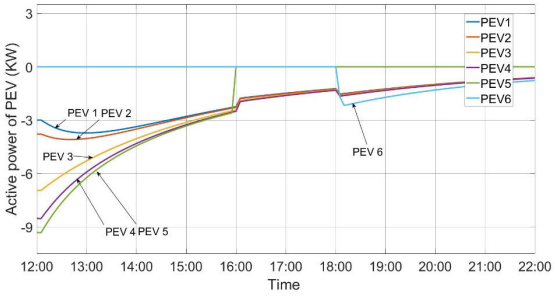


**FIGURE 16.** Active power of PEV work in V2G mode.

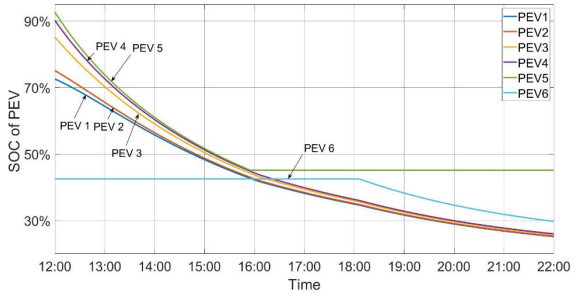


**FIGURE 17.** SOC of PEV work in V2G mode.

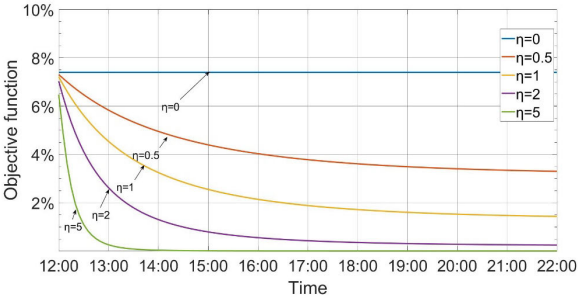


**FIGURE 18.** Relationship between balance parameter and objective function.

decreases faster as the power balance parameter $\eta$ increases within the range of values.

FIGURE 19 shows the effect of the energy management system on the load curve. In this simulation, the aggregator with the proposed energy management system replace 30% of the PEV load, and the simulation based on actual data from paper [25]. The simulation starts at 12:00 and ends at 22:00. The baseload is not affected by PEVs load. The maximum value of the PEV load without energy management is 173kw, the minimum value is 115kW, and the coefficient of variation is 12.9%. The maximum value of the PEV load with energy management is 147kw, the minimum value is 128kW, and the coefficient of variation is 3.7%. The proposed energy management system reduces PEVs load fluctuations. The peak of the PEVs+base load curve with proposed energy management is 299kw and that without energy management is 324kw. The proposed energy management allows for the

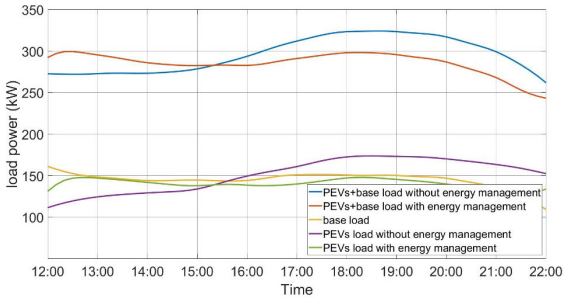


**FIGURE 19.** The power load curve with energy management.

**TABLE 1.** Parameters in experiment.

| Description | Value |
|---|---|
| Maximum power rating in V2G/G2V | 500W |
| Battery voltage | 110V |
| Input voltage frequency | 50Hz |
| Switching frequency $f_s$ | 10KHz |
| Rated power of PMSM | 3.8KW |
| Stator inductance of PMSM | 1mH |
| Pole number of PMSM | 6 |
| Current rating of the PMSM | 10A |

orderly charging of the PEVs and reduces the peak of the load curve.

### B. EXPERIMENTAL RESULTS

To verify the proposed EDROC, a workbench is built as shown in FIGURE 20. A permanent magnet synchronous motor is used as the AC-side power inductor in V2G/G2V mode. The amplitude of the voltage of the AC source is set at 60V. The Rohm SCT3120AL MOSFET switches and AACPL-W346 gate driver optocouplers were used to building the switching network, the voltage hall sensors CHV-25P/500, the current hall sensors CHB-15AD, and the Texas Instruments ADS8556 were used to build the sampling circuit. An STM32G484 microprocessor controller is utilized to implement the proposed vehicle level control with a switching frequency of 10 kHz.The parameters in the experiment as shown in Table 1.

In this experiment, the proportional and integral constant of AC current controller is set to 0.6 and 500, respectively; The proportional and integral constant of the battery voltage controller is set to 0.15 and 150, respectively. The bandwidth of the battery voltage controller set is to 218 rad/s which is lower than the resonant frequency of the AC current controller(314rad/s); The bandwidth of the active power controller is set to 20 rad/s which is one order of magnitude smaller than that of battery voltage controller. The bandwidth of the active power controller is set to 43 rad/s to avoid conflicts between controllers. The phase margin of all controllers is set to more than 90 degrees to reduce overshoot in vehicle level. The experiment using the parameters in Table 2.

The experimental operating state of the EDROC is shown in Chapter II. The switches $S_1$, $S_2$, $S_3$ and $S_6$ are disabled; the

**TABLE 2.** Parameters for controllers.

| Parameter | battery voltage controller | active power controller | reactive power controller | AC current controller |
|---|---|---|---|---|
| proportional constant | 0.15 | 0.5 | 0.1 | 0.6 |
| integral constant | 150 | 10 | 30 | 500 |
| phase margin(deg) | 98.6 | 120.0 | 95.7 | 129.2 |
| bandwidth(rad/s) | 218 | 20 | 43 | / |
| resonant frequency(rad/s) | / | / | / | 314 |

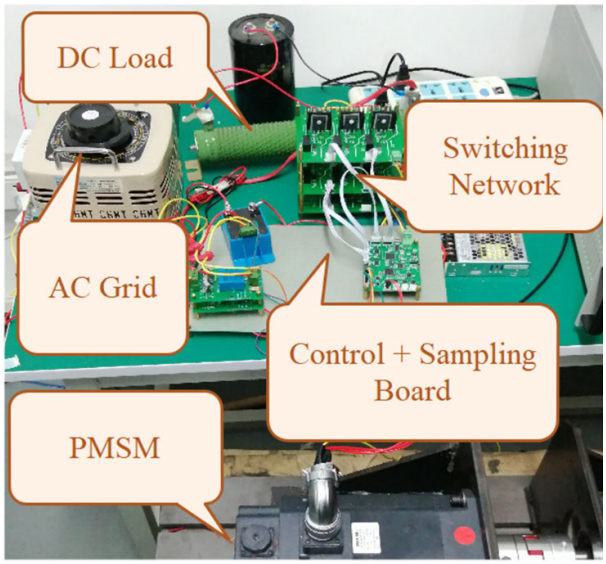


**FIGURE 20.** Workbench of the proposed EDROC.

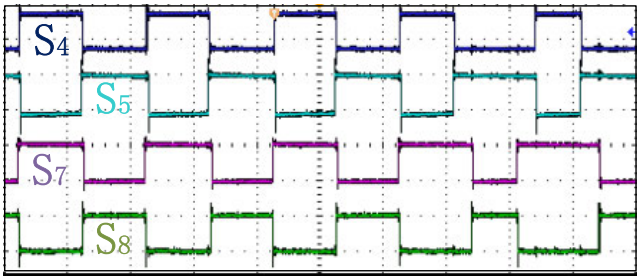


**FIGURE 21.** The PWM wave of EDROC.

switches $S_4$, $S_5$, $S_7$ and $S_8$ are controlled by the PWM which modulation via STM32G474, as shown in FIGURE 21.

FIGURE 22 shows the voltage of AC source waveforms and three-phase inductive current waveforms of PMSM.A-phase current has the same fundamental frequency and phase as the voltage waveforms of AC source, and the amplitude of A- Phase current is 2A. The A- Phase current is equal to the sum of B-phase current and C-phase current.

FIGURE 23 and FIGURE 24 show the voltage and the current of AC source in G2V mode and V2G mode, respectively. The proposed converter can control the direction of energy flow with the proposed control strategy.

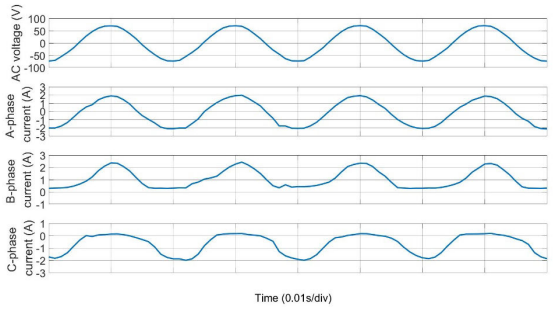


**FIGURE 22.** Inductive current waveforms of PMSM.

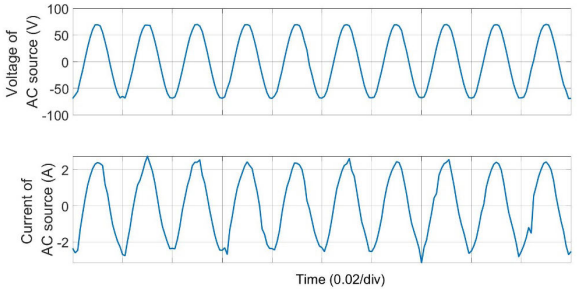


**FIGURE 23.** The voltage of AC source and the current of AC source in G2V mode.

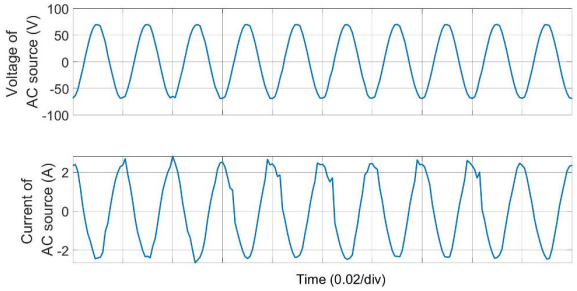


**FIGURE 24.** The voltage of AC source and the current of AC source in V2G mode.

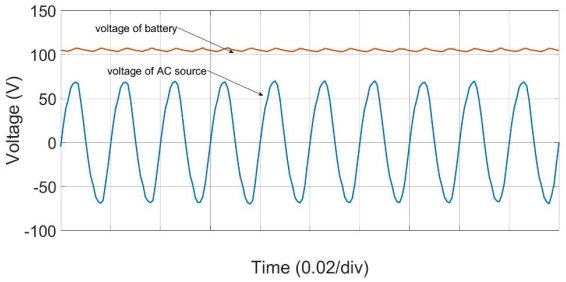


**FIGURE 25.** Relationship between the voltage of the AC source and the voltage of the battery.

FIGURE 25 shows the relationship between the voltage of the AC source and the voltage of the battery. The voltage of the battery is 110V, and the amplitude of the AC voltage is 60V. This relationship satisfies equation (5) and the voltage of the battery can be controlled.

**TABLE 3.** Comparison to on-board converter.

| on-board converter | multifunction | Additional inductance | Specially designed motor | Number of power switches |
|---|---|---|---|---|
| The proposed EDROC | Y | N | N | 8 |
| The EDROC in [5] | Y | N | Y | 12 |
| The EDROC in [6] | Y | N | Y | 8 |
| The EDROC in [26] | Y | N | N | 10 |
| The sing-phase charger in [27] | N | Y | / | 4 |
| The motor-driven converter in [28] | N | / | N | 6 |

NOTE: Y is YES, N is NO,

### C. THE HARDWARE COST COMPARISON OF EDROC

The EDROC reduces the hardware cost by replacing the additional inductance with a PMSM in V2G/G2V mode and integrates the functions of the charger and the drive system to reduce the number of switches (Compared to the PEV with independent charging systems and drive systems). The proposed EDROC further reduces the number of switching tubes by optimizing the topology and does not configurator specially designed motors. The proposed EDROC has a lower hardware cost compared to other EDROCs or chargers and reducing the hardware cost of V2G/G2V applications. The hardware cost comparison of EDROC as shown in Table 3.

## V. CONCLUSION

This article proposes a hierarchical control strategy with a novel EDROC which can be onboard and directly utilize the power outlet at the office or home. The experiments show that the proposed EDROC enables the bidirectional flow of energy to meets the requirements of V2G/G2V systems. The proposed control strategy achieves the reasonable distribution of energy between the PEVs under a hierarchical control structure. The simulations show that the V2G/G2V system which controlled under the proposed control strategy avoids overcharging, and reduces the dispersion of PEV SOC. The application of the V2G/G2V energy management system proposed in this article can reduce the hardware cost of charging PEVs and make efficient use of energy.

## REFERENCES

[1] T. Harighi, R. Bayindir, S. Padmanaban, L. Mihet-Popa, and E. Hossain, "An overview of energy scenarios, storage systems and the infrastructure for vehicle-to-grid technology," *Energies*, vol. 11, no. 8, p. 2174, Aug. 2018.

[2] M. Huda, T. Koji, and M. Aziz, "Techno economic analysis of vehicle to grid (V2G) integration as distributed energy resources in Indonesia power system," *Energies*, vol. 13, no. 5, p. 1162, 2020.

[3] S. B. Peterson, J. F. Whitacre, and J. Apt, "The economics of using plug-in hybrid electric vehicle battery packs for grid storage," *J. Power Sources*, vol. 195, no. 8, pp. 2377–2384, Oct. 2010.

[4] M. Yilmaz and P. T. Krein, "Review of battery charger topologies, charging power levels, and infrastructure for plug-in electric and hybrid vehicles," *IEEE Trans. Power Electron.*, vol. 28, no. 5, pp. 2151–2169, May 2013.

[5] F. Yu, W. Zhang, Y. Shen, and J. Mao, "A nine-phase permanent magnet electric-drive-reconstructed onboard charger for electric vehicle," *IEEE Trans. Energy Convers.*, vol. 33, no. 4, pp. 2091–2101, Dec. 2018.

[6] Z. Wang, Y. Zhang, S. You, H. Xiao, and M. Cheng, "An integrated power conversion system for electric traction and V2G operation in electric vehicles with a small film capacitor," *IEEE Trans. Power Electron.*, vol. 35, no. 5, pp. 5066–5077, May 2020, doi: 10.1109/TPEL.2019.2944276.

[7] L. Wang, Y. Wan, W. Cao, and C. Fan, "Optimizing strategy of spatial orderly charging for EVs based on complex network theory," in *Proc. Chin. Automat. Congr. (CAC)*, Hangzhou, China, Nov. 2019, pp. 1536–1541, doi: 10.1109/CAC48633.2019.8997488.

[8] S. Ge, J. Yan, and H. Liu, "Ordered charging optimization of electric vehicles based on charging load spatial transfer," in *Proc. 22nd Int. Conf. Electr. Mach. Syst. (ICEMS)*, Harbin, China, Aug. 2019, pp. 1–6, doi: 10.1109/ICEMS.2019.8922218.

[9] B. Yun and L. Xiao, "A method for orderly charging electric vehicles applied to residential quarter," in *Proc. 3rd Int. Conf. Adv. Electron. Mater., Comput. Softw. Eng. (AEMCSE)*, Shenzhen, China, Apr. 2020, pp. 861–867, doi: 10.1109/AEMCSE50948.2020.00186.

[10] L. P. Fernandez, T. G. S. Roman, R. Cossent, C. M. Domingo, and P. Frias, "Assessment of the impact of plug-in electric vehicles on distribution networks," *IEEE Trans. Power Syst.*, vol. 26, no. 1, pp. 206–213, Feb. 2011, doi: 10.1109/TPWRS.2010.2049133.

[11] X. Chen, K.-C. Leung, A. Y. S. Lam, and D. J. Hill, "Online scheduling for hierarchical vehicle-to-grid system: Design, formulation, and algorithm," *IEEE Trans. Veh. Technol.*, vol. 68, no. 2, pp. 1302–1317, Feb. 2019.

[12] N. Jabalameli, X. Su, and A. Ghosh, "Online centralized charging coordination of PEVs with decentralized var discharging for mitigation of voltage unbalance," *IEEE Power Energy Technol. Syst. J.*, vol. 6, no. 3, pp. 152–161, Sep. 2019.

[13] U. C. Chukwu and S. M. Mahajan, "Real-time management of power systems with V2G facility for smart-grid applications," *IEEE Trans. Sustain. Energy*, vol. 5, no. 2, pp. 558–566, Apr. 2014.

[14] M. J. E. Alam, K. M. Muttaqi, and D. Sutanto, "Effective utilization of available PEV battery capacity for mitigation of solar PV impact and grid support with integrated V2G functionality," *IEEE Trans. Smart Grid*, vol. 7, no. 3, pp. 1562–1571, May 2016.

[15] K. Kaur, A. Dua, A. Jindal, N. Kumar, M. Singh, and A. Vinel, "A novel resource reservation scheme for mobile PHEVs in V2G environment using game theoretical approach," *IEEE Trans. Veh. Technol.*, vol. 64, no. 12, pp. 5653–5666, Dec. 2015.

[16] N. Rahbari-Asr, M.-Y. Chow, J. Chen, and R. Deng, "Distributed real-time pricing control for large-scale unidirectional V2G with multiple energy suppliers," *IEEE Trans. Ind. Informat.*, vol. 12, no. 5, pp. 1953–1962, Oct. 2016.

[17] L. Zhang, H. Ma, D. Shi, P. Wang, G. Cai, and X. Liu, "Reliability oriented modeling and analysis of vehicular power line communication for vehicle to grid (V2G) information exchange system," *IEEE Access*, vol. 5, pp. 12449–12457, 2017.

[18] N. Saxena and B. J. Choi, "Authentication scheme for flexible charging and discharging of mobile vehicles in the V2G networks," *IEEE Trans. Inf. Forensics Security*, vol. 11, no. 7, pp. 1438–1452, Jul. 2016.

[19] F. Barrero-González, M. I. Milanés-Montero, E. González-Romera, E. Romero-Cadaval, C. Roncero-Clemente, "Control strategy for electric vehicle charging station power converters with active functions," *Energies*, vol. 12, no. 20, p. 3971, 2019.

[20] H. Han, D. Huang, D. Liu, and Q. Li, "Autonomous frequency regulation control of V2G(vehicle-to-grid) system," in *Proc. 29th Chin. Control Decis. Conf. (CCDC)*, Chongqing, China, May 2017, pp. 5826–5829, doi: 10.1109/CCDC.2017.7978208.

[21] L. Chen, Y. Jiang, X. Li, L. Yao, X. Xu, and T. Geng, "Frequency regulation strategy for decentralized V2G control," in *Proc. 5th Int. Conf. Electric Utility Deregulation Restructuring Power Technol. (DRPT)*, Changsha, China, Nov. 2015, pp. 2626–2629, doi: 10.1109/DRPT.2015.7432692.

[22] D. Liu, Q. Zhong, Y. Wang, and G. Liu, "Modeling and control of a V2G charging station based on synchronverter technology," *CSEE J. Power Energy Syst.*, vol. 4, no. 3, pp. 326–338, Sep. 2018, doi: 10.17775/CSEE-JPES.2016.01430.

[23] P. Yang, T. Peng, H. Wang, H. Han, J. Yang, and H. Wang, "A single-phase current-source bidirectional converter for V2G application," in *Proc. IEEE 3rd Int. Future Energy Electron. Conf. ECCE Asia (IFEEC-ECCE Asia)*, Kaohsiung, Taiwan, Jun. 2017, pp. 704–709, doi: 10.1109/IFEEC.2017.7992125.

[24] M. C. Kisacikoglu, M. Kesler, and L. M. Tolbert, "Single-phase on-board bidirectional PEV charger for V2G reactive power operation," *IEEE Trans. Smart Grid*, vol. 6, no. 2, pp. 767–775, Mar. 2015.

[25] M. Muratori, M. C. Roberts, R. Sioshansi, V. Marano, and G. Rizzoni, "A highly resolved modeling technique to simulate residential power demand," *Appl. Energy*, vol. 107, pp. 465–473, Jul. 2013.

[26] C. Shi, Y. Tang, and A. Khaligh, "A single-phase integrated onboard battery charger using propulsion system for plug-in electric vehicles," *IEEE Trans. Veh. Technol.*, vol. 66, no. 12, pp. 10899–10910, Dec. 2017, doi: 10.1109/TVT.2017.2729345.

[27] L. Jing, X. Wang, B. Li, M. Qiu, B. Liu, and M. Chen, "An optimized control strategy to improve the current zero-crossing distortion in bidirectional AC/DC converter based on V2G concept," in *Proc. Int. Power Electron. Conf. (IPEC-Niigata -ECCE Asia)*, Niigata, Japan, May 2018, pp. 878–882, doi: 10.23919/IPEC.2018.8507917.

[28] J. Wu, J. Wang, C. Gan, Q. Sun, and W. Kong, "Efficiency optimization of PMSM drives using field-circuit coupled FEM for EV/HEV applications," *IEEE Access*, vol. 6, pp. 15192–15201, 2018, doi: 10.1109/ACCESS.2018.2813987.

[29] X. Bai and W. Qiao, "Robust optimization for bidirectional dispatch coordination of large-scale V2G," *IEEE Trans. Smart Grid*, vol. 6, no. 4, pp. 1944–1954, Jul. 2015.

[30] K.-W. Hu, P.-H. Yi, and C.-M. Liaw, "An EV SRM drive powered by battery/supercapacitor with G2V and V2H/V2G capabilities," *IEEE Trans. Ind. Electron.*, vol. 62, no. 8, pp. 4714–4727, Aug. 2015.

[31] H. Liu, H. Ning, Y. Zhang, and M. Guizani, "Battery status-aware authentication scheme for V2G networks in smart grid," *IEEE Trans. Smart Grid*, vol. 4, no. 1, pp. 99–110, Mar. 2013.

[32] J. Ye, C. Shi, and A. Khaligh, "Single-phase charging operation of a three-phase integrated onboard charger for electric vehicles," in *Proc. IEEE Transp. Electrific. Conf. Expo (ITEC)*, Long Beach, CA, USA, Jun. 2018, pp. 681–686.

[33] C. Shi, Y. Tang, and A. Khaligh, "A three-phase integrated onboard charger for plug-in electric vehicles," *IEEE Trans. Power Electron.*, vol. 33, no. 6, pp. 4716–4725, Jun. 2018.

[34] V. Verma and A. Kumar, "Smart parking for PHEV/EV using solid state split voltage bidirectional converter at UPF with V2G/G2V capability," in *Proc. IEEE Int. Conf. Power Electron., Drives Energy Syst. (PEDES)*, Trivandrum, India, Dec. 2016, pp. 1–6, doi: 10.1109/PEDES.2016.7914525.

[35] D. Das, N. Weise, K. Basu, R. Baranwal, and N. Mohan, "A bidirectional soft-switched DAB-based single-stage three-phase AC–DC converter for V2G application," *IEEE Trans. Transport. Electrific.*, vol. 5, no. 1, pp. 186–199, Mar. 2019, doi: 10.1109/TTE.2018.2886455.

[36] M. Kwon and S. Choi, "An electrolytic capacitorless bidirectional EV charger for V2G and V2H applications," *IEEE Trans. Power Electron.*, vol. 32, no. 9, pp. 6792–6799, Sep. 2017, doi: 10.1109/TPEL.2016.2630711.

[37] F. Li, F. Ji, H. Guo, H. Li, and Z. Wang, "Research on integrated bidirectional control of EV charging station for V2G," in *Proc. 2nd Int. Conf. Power Renew. Energy (ICPRE)*, Chengdu, China, Sep. 2017, pp. 833–838, doi: 10.1109/ICPRE.2017.8390651.

[38] B. Li, L. Jing, X. Wang, N. Chen, B. Liu, and M. Chen, "A smooth mode-switching strategy for bidirectional OBC base on V2G technology," in *Proc. IEEE Appl. Power Electron. Conf. Exposit. (APEC)*, Anaheim, CA, USA, Mar. 2019, pp. 3320–3324, doi: 10.1109/APEC.2019.8721774.

[39] Q. Sun, S. Fu, H. Lv, S. Gao, and K. Wei, "Study on bidirectional PWM converter considering robustness of PR controller for V2G application," in *Proc. IEEE Int. Conf. Appl. Supercond. Electromagn. Devices (ASEMD)*, Tianjin, China, Apr. 2018, pp. 1–2, doi: 10.1109/ASEMD.2018.8558903.

[40] Y. Ye, M. Kazerani, and V. H. Quintana, "A novel modeling and control method for three-phase PWM converters," in *Proc. IEEE 32nd Annu. Power Electron. Spec. Conf.*, Vancouver, BC, Canada, vol. 1, Jun. 2001, pp. 102–107, doi: 10.1109/PESC.2001.954002.

[41] Y. Zhang, W. Xie, and Y. Zhang, "Deadbeat direct power control of three-phase pulse-width modulation rectifiers," *IET Power Electron.*, vol. 7, no. 6, pp. 1340–1346, Jun. 2014, doi: 10.1049/iet-pel.2013.0563.

[42] Y. Han, M. Luo, X. Zhao, J. M. Guerrero, and L. Xu, "Comparative performance evaluation of orthogonal-signal-generators-based single-phase PLL algorithms—A survey," *IEEE Trans. Power Electron.*, vol. 31, no. 5, pp. 3932–3944, May 2016, doi: 10.1109/TPEL.2015.2466631.

**SHUO LIU** received the Ph.D. degree in electrical engineering from Beijing Jiaotong University, Beijing, China, in 2015. He is currently an Associate Professor with the Electrical and Control Engineering College, North China University of Technology, Beijing. His research interests include Z-source converter, matrix converter, and motor drives.

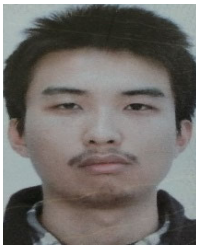

**DIXI XIN** is currently pursuing the M.S. degree in electrical engineering with the Electrical and Control Engineering College, North China University of Technology, Beijing. His current interests include bidirectional converter and electric vehicles.

**LIYONG YANG** is currently an Associate Professor with the Electrical and Control Engineering College, North China University of Technology, Beijing. His current research interests include electrical machine drives and power electronics.

**JIANLIN LI** (Member, IEEE) was born in 1976. His current research interests include grid-connected inverters control technology, the impact of distributed generation on power quality, and micro-grid control technology.

**LI WANG** (Member, IEEE) received the Ph.D. degree in precision instruments and machinery from Beihang University, Beijing, China, in 2004. From 2004 to 2006, he was a Postdoctoral Researcher with Beihang University. He is currently the Dean of the School of Electrical and Control Engineering, North China University of Technology University, Beijing. His research interests include intelligent traffic signal control and traffic simulation, Internet of Vehicles, and artificial intelligence.